Shape modification of III-V nanowires: The role of nucleation on sidewalls

V. G. Dubrovskii,[1,2,*] N. V. Sibirev,[1] G. E. Cirlin,[1,2,3] M. Tchernycheva,[4] J. C. Harmand,[3] and V. M. Ustinov[1,2]

[1]*St.-Petersburg Physical Technological Centre of the Russian Academy of Sciences for Research and Education, Khlopina 8/3, 195220, St.-Petersburg, Russia*

[2]*Ioffe Physical Technical Institute of the Russian Academy of Sciences, Politekhnicheskaya 26, 194021, St.-Petersburg, Russia*

[3]*CNRS-LPN, Route de Nozay, 91460 Marcoussis, France*

[4]*Department OptoGaN, Institut d'Electronique Fondamentale, UMR 8622 CNRS, Université Paris-Sud, 91405 Orsay Cedex, France*

(Received 14 September 2007; revised manuscript received 18 January 2008; published 14 March 2008)

The effect of sidewall nucleation on nanowire morphology is studied theoretically. The model provides a semiquantitative description of nanowire radius as a function of its length and the distance from the surface. It is demonstrated that the wire shape critically depends on the diffusion flux of adatoms from the substrate and on the rate of direct impingement to the sidewalls. At high diffusion flux the wire shape is cylindrical. A decrease of diffusion from the surface leads to the onset of nucleation on the sidewalls resulting in the lateral extension and in the reduction of wire length. The wire shape changes from cylindrical to conical, because the supersaturation of adatoms driving the nucleation is higher at the wire foot than at the top. It is shown that the shape modification becomes pronounced at low growth temperatures. Theoretical results are used to model the experimentally observed shapes of GaAs and GaP wires, grown by Au-assisted molecular beam epitaxy at different temperatures.

DOI: 10.1103/PhysRevE.77.031606 PACS number(s): 81.10.Aj, 68.70.+w

I. INTRODUCTION

Semiconductor nanowires have recently gained a continuously growing interest due to many promising applications in nanoelectronic, nanophotonic, and nanosensing devices [1–4], as well as from the viewpoint of fundamental growth processes [5–12]. Radius and position controlled growth has been considered as one of the most attractive features for fabrication of organized arrays of wires, beginning from the early works on micrometer scale whiskers [13,14] and ending up with the recent developments at the nanometer scale [1–4]. Modern epitaxial techniques enable the fabrication of nanowires with radii of the order of 10 nanometers and lengths typically of several micrometers. Growth of Si [5] and III-V [6–10,12,15] nanowires is driven mainly by the adatom diffusion from the substrate surface and from the sidewalls. Despite very impressive progress in nanowire fabrication, many growth-related aspects in this field are not completely understood so far. In particular, for the controlled production of nanowires it is important to investigate the effects influencing their geometrical shape.

Ideally, III-V wires obtained on the (111) surfaces activated by the seed drops should grow perpendicular to the surface with a constant radius defined by the size of the drop. However, many recent studies reveal that the wire radius varies during the growth. Taking as an example the case of Au-assisted molecular beam epitaxy (MBE) of GaAs wires, the temperature domain for wire formation via the vapor-liquid-solid mechanism [13] ranges from 420 to 620 °C [7–10,16,17]. Wires obtained at higher temperatures, $T>500$ °C, grow with constant radius during the first several micrometers of their length. At $T=580$ °C such uniform growth is observed until the length exceeds 3 μm [8,17]. Longer wires are tapered towards their top because of the reevaporation of some material from the sidewalls. This effect is described in Ref. [8] and modeled in Ref. [10]. At lower $T\sim 420-500$ °C, the wires become considerably shorter and develop a specific conical shape [16,17]. In this case, the size of the drop remains constant. Experimental facts strongly suggest that the observed conicity is explained either by some changes at the liquid-solid interface (e.g., in the contact angle and in the direction of interfacial forces [18,19]) or by the nucleation of adatoms on the sidewalls before they reach the top. The latter effect was mentioned as technologically undesirable in the book by Givargizov [14], where it was also argued that the lateral growth usually occurs at low temperatures. This observation is supported by the above-mentioned findings for GaAs wires. To the best of our knowledge, there was no attempt made so far to master the effect of sidewall nucleation theoretically. It is not a simple problem because relevant theoretical models must include nonlinear terms for two reasons. First, the nucleation rate depends exponentially on the supersaturation through the Zel'dovich equation of classical nucleation theory [20]. Second, the side facets of laterally growing wires are no longer flat, while the local curvature of the surface will itself depend on the nucleation rate.

This paper aims at modeling the wire growth in both the vertical and lateral directions. The model is capable of describing the wire radius as a function of its length and the distance from the surface. We propose a nonlinear equation for the adatom supersaturation on the sidewalls of the "diffusion plus reaction type." A simplified version is reduced to a nonlinear differential equation with a constant rate of "birth" and an exponential "extinction" of particles, which can be treated analytically. Our analysis shows that in the case of beam deposition there exists a certain critical diffusion flux, below which the diffusion-induced growth should be stopped completely, i.e., the crystals would emerge in the form of laterally extending islands rather than wires. Nu-

*dubrovskii@mail.ioffe.ru

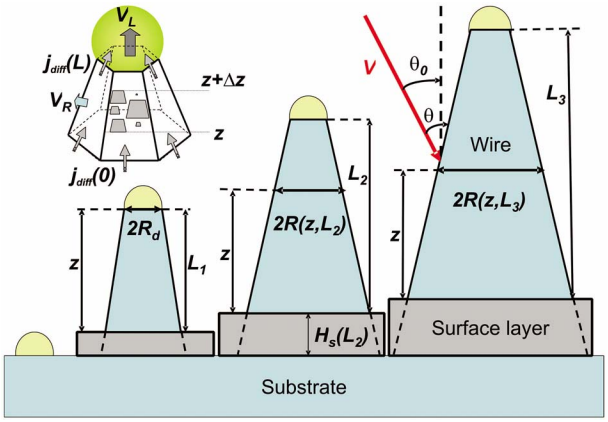

FIG. 1. (Color online) Schematics of the growth model including the wire, the surface layer, and the drop, at three different times. J is the impingement flux, θ_0 is the incident angle of the beam to the flat surface, and θ is the local incident angle. The inset at the top left illustrates the polynuclear lateral growth of the side facet.

merical simulations are used to analyze our experimental data for the Au-assisted MBE of GaAs and GaP nanowires.

II. MODEL

Our model is the following. Consider a wire growing with arbitrary shape characterized by radius $R(z,t)$ and length $L(t)$, where z is the distance from the surface layer ("height") and t is the time (Fig. 1). Obviously, point $z=0$ corresponds to the wire foot and point $z=L(t)$ to the top. At $t=0$ the drop of radius R_d is on the surface of a bare substrate and the wire length $L(t=0)=0$. We assume that the radius of the drop remains constant during the growth, implying $R[z,L(t)=z]=R_d$. The wire cross section is assumed to be a circle or a regular polygon; in the latter case $R(z,t)$ is the radius of the circle inscribed in the polygon. Vertical and lateral growth of the wire is described by the following equations:

$$\frac{dL}{dt} = V_L(L), \quad L(t=0)=0, \tag{1}$$

$$\frac{dR(z,t)}{dt} = V_R(z,L), \quad R[z,L(t)=z]=R_d, \tag{2}$$

where V_L and V_R are, by definition, the vertical and lateral growth rates, respectively. In the steady state, the radius R can be treated as function of z and L instead of z and t, by using the one-to-one correspondence between L and t. In this case Eqs. (1) and (2) are reduced to

$$R(z,L) = R_d + \int_z^L dL' \frac{V_R(z,L')}{V_L(L')}. \tag{3}$$

For the following analysis we require some models for the vertical and lateral growth rates. As usually admitted, the vertical growth rate in the diffusion-induced mode depends on the equivalent deposition rate $V=J\Omega\cos\theta_0$ (θ_0 is the incident angle of the beam, see Fig. 1), the desorption from the drop, the growth rate of surface layer, and the diffusion-induced contribution [7],

$$V_L(L) = (\varepsilon-\gamma)V + \frac{\Omega}{\pi R_d^2} j_{diff}(L). \tag{4}$$

The parameter γ is the rate of desorption from the drop in units of V [7], Ω is the volume per III-V pair in the crystal, and parameter $\varepsilon=1-V_s/V$ accounts for the vertical growth of the surface layer at rate V_s. The diffusion flux of adatoms to the top, driven by the difference of chemical potentials on the surface layer and in the drop [10] (or on the top facet [15] in the case of catalyst-free growth), is defined as

$$j_{diff}(L) = -2\pi R_d D \left.\frac{dn}{dz}\right|_{z=L}. \tag{5}$$

Here, D is the diffusion coefficient on the sidewalls and n is the adatom concentration. The flux given by Eq. (5) generally consists of two fluxes, one resulting from the atoms directly impinging on the sidewalls and another formed by the atoms impinging on the surface, then migrating to the wire base and finally to its top along the sidewalls. While considering the latter we assume that the flux to the wire base per unit length of the base $2\pi R_0$ remains constant during the growth. As shown in Ref. [21], this is always true if R_0 is much larger than the effective diffusion length of adatoms on the surface λ_s. Our boundary condition should hold for a sufficiently thick wire foot with $R_0>100$ nm, because the diffusion on the surface is limited by the nucleation and the values of λ_s estimated for typical growth conditions during MBE of Ga(Al)As wires are of the order of few tens of nm [22]. Using the equation of continuity at the wire foot, we obtain

$$-D \left.\frac{dn}{dz}\right|_{z=0} = \frac{j_{diff}(0)}{2\pi R_0} = \text{const}. \tag{6}$$

Nucleation-mediated lateral growth of the wire may proceed in mononuclear or polynuclear mode, depending on the drop radius and the growth conditions [20,23]. For the sake of simplicity, also taking into consideration that the effect of nucleation is pronounced at high supersaturations of adatoms, below we use the radius independent expression for V_R in the polynuclear mode [20]

$$V_R(\eta) = h[I(\eta)v^2(\eta)]^{1/3}. \tag{7}$$

Here, h is the height of a monolayer, I is the nucleation rate, and v is the lateral growth rate of a two-dimensional island. Functions I and v depend on the adatom supersaturation, defined as $\eta=n/n_{eq}-1$. The equilibrium concentration of adatoms n_{eq} is determined by the temperature T, further assumed as being constant along the wire, which is always fulfilled for sufficiently short wires with a length of several μm [11]. The dependence of V_R on η is mainly governed by a very steep exponential dependence of I on η [20,23,24]:

$$I(\eta) \propto \tau_D^{-1} \exp\left[-\frac{a}{\ln(\eta+1)}\right]. \tag{8}$$

The expression for the nucleation barrier is written in the case of two-dimensional nuclei arising at the solid-vapor in-

terface [23]; $a \equiv c\sigma(\psi_{SV}/k_BT)^2$ is a thermodynamic constant, σ is the area of adsorption site on the sidewalls, ψ_{SV} is the specific edge energy of the lateral solid-vapor interface per unit length of the island, c is the island shape constant, and k_B is the Boltzmann constant. Parameter τ_D describes the characteristic time of island growth.

Steep exponential dependence of the nucleation rate on the supersaturation allows one to simplify Eq. (7) to the form [23,24]

$$V_R(U) \cong V_R(0)\exp(-U). \tag{9}$$

Here, the new unknown function is defined as $U=(\Gamma/3)\times[(\eta_0-\eta)/\eta_0]$. The parameter Γ, obtained simply from the Taylor expansion of $F(\eta)$ near η_0, has the same order of magnitude as the critical size of classical nucleation theory at $\eta=\eta_0$ [24] and is therefore much larger than unity. Quantities $V_R(0)$ and η_0 are the lateral growth rate and the adatom supersaturation at the wire foot, respectively. When the adatom diffusion flux is directed towards the wire top, η must decrease with the height. Therefore, we are looking for the solutions for U increasing with z.

Finally, the steady state kinetic equation for the adatom concentration $n(z)$ on the curved surface of local radius $R(z,L)$ is

$$-\frac{d}{dz}\left[2\pi RD\frac{dn}{dz}\right] = 2\pi R\left[J_{eff} - \frac{n}{\tau_A} - \frac{V_R}{\Omega}\right]. \tag{10}$$

The left-hand side describes the diffusion, the first term in the right-hand side stands for the adsorption on the sidewalls, the second term describes the desorption from the sidewalls with a characteristic lifetime τ_A, and the third term gives the adatom sink due to the nucleation. The effective impinging flux at height z in the case of beam deposition is determined as $J_{eff}=(V/\pi\Omega)\sin\theta/\cos\theta_0$, where $\theta=\theta_0+\Delta\theta$ is the local incident angle and $\Delta\theta$ is the adjunct caused by the curvature of the surface, as shown in Fig. 1. From geometrical considerations, the latter is given by $\tan\Delta\theta=-dR/dz$. Using Eqs. (4)–(6) and (9), Eqs. (10) and (3) for n and R can be rewritten in terms of the unknown U in the form

$$\frac{d^2U}{dx^2} + \frac{1}{\rho}\frac{d\rho}{dx}\frac{dU}{dx} = -e^{-U} + \frac{V}{\pi V_R(0)}\frac{\sin(\theta_0+\Delta\theta)}{\cos\theta_0}, \tag{11}$$

$$U(x=0)=0, \qquad \left.\frac{dU}{dx}\right|_{x=0} = \sqrt{A}, \tag{12}$$

$$\rho(x,l) = 1 + \frac{e^{-U(x)}}{2}\int_x^l \frac{dx'}{dU/dx' + \nu}. \tag{13}$$

Here, the normalized radius $\rho=R/R_d$ and the normalized vertical coordinates $x=z/L_*$; $l=L/L_*$ are expressed in the units of the effective diffusion length on the sidewalls, given by

$$L_* = \left[\frac{3\Omega D n_{eq}\eta_0}{V_R(0)\Gamma}\right]^{1/2}. \tag{14}$$

Since L_* is always much smaller than the diffusion length of a single adatom on the flat lateral surface λ [3–10 μm in the case of Ga atoms on the GaAs(110) surface at 580 °C [8,25]], in Eq. (11) we do not write the term which is proportional to $(L_*/\lambda)^2$. The normalized diffusion flux to the wire base equals

$$\sqrt{A} = \frac{\Gamma}{3Dn_{eq}\eta_0}\frac{j_{diff}(0)}{2\pi R_0}L_*. \tag{15}$$

The local curvature of the surface in the right-hand side of Eq. (11) is obtained from

$$\tan\Delta\theta = -\frac{R_d}{L_*}\frac{d\rho}{dx}.$$

The constant $\nu=[(\varepsilon-\gamma)VR_d]/[2V_R(0)L_*]$ in Eq. (13) stands for the adsorption induced contribution to the vertical growth rate.

In these nondimensional coordinates, the wire shape depends on the diffusion flux to the base $\sqrt{A}$ and the adsorption-desorption coefficient ν. The solution to Eq. (11) for U with boundary conditions (12) is used in Eq. (13) for computing the wire shape. The nonlinear equation for $\rho(x,l)$ given by Eqs. (11)–(13) in its general form can only be solved numerically. Simulation results will be presented below. In Sec. III we show that a simplified version of the model can be studied analytically. This study enables us to draw several qualitative conclusions regarding the behavior of wire shape at different growth conditions.

III. ANALYTICAL SOLUTION

Let us now consider the simplified version of Eq. (11) at a small curvature of the surface, setting the local incident angle θ to θ_0. The resulting two-parametric equation describes the diffusion with the constant rate of birth and the exponential rate of extinction at the fixed particle supplying flux at $x=0$,

$$d^2U/dx^2 = -\exp(-U) + \beta,$$

$$U(x=0)=0; \quad U'(x=0)=\sqrt{A}. \tag{16}$$

Here, the parameter $\beta=[V\tan\theta_0]/[\pi V_R(0)]$ represents the direct impingement to the sidewalls, while $U'(0)=\sqrt{A}$, as above, stands for the adatom supply at the wire foot. Equation (16) has the first integral of the form

$$\frac{1}{2}\left(\frac{dU}{dx}\right)^2 + G(U) = \frac{A}{2} \tag{17}$$

with

$$G(U) = 1 - \beta U - \exp(-U). \tag{18}$$

We now show how the main properties of the system at different values of A and β can be analyzed by considering Eqs. (17) and (18). It is noteworthy that Eq. (17) has the form of the energy conservation equation for a classical point "particle" with "coordinate" U, "time" x, "total energy" $A/2=$const, "potential energy" $G(U)$ and a unit "mass." The total energy is defined by $U'(0)$ and the form of the potential

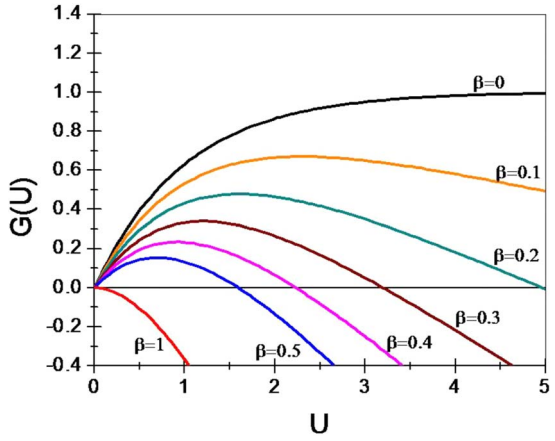

FIG. 2. (Color online) Forms of potential $G(U)$ at different β.

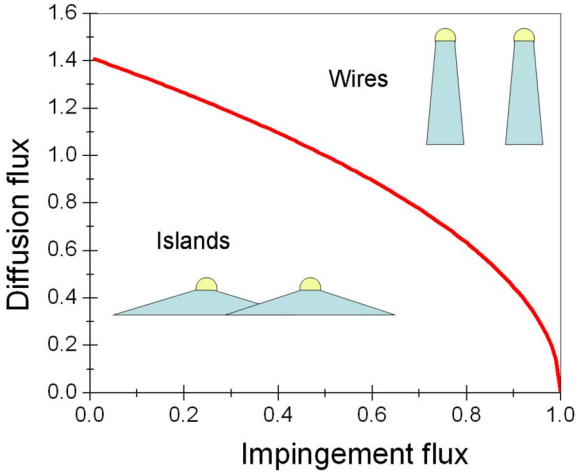

FIG. 3. (Color online) Kinetic phase diagram illustrating the domains for the island and the wire formation.

depends on β. Initial conditions to Eq. (16) yield that our hypothetic particle has zero coordinate and the fixed velocity $U'(0)$ at zero time. As already mentioned, relevant solutions for $U(x)$ must increase with x, since the diffusion flux would otherwise change its direction. In terms of particle motion we are therefore searching for the cases when the particle, starting its motion at $U=0$ with given velocity, travels to point $U=+\infty$ at $x\to\infty$. Such unlimited motion takes place only if $A/2$ is larger than the potential barrier, which equals the maximum of $G(U)$ at $U=U_*$. The values of U_* and $G(U_*)$ are readily calculated by maximizing Eq. (18): $U_*=-\ln\beta$, $G(U_*)=1-\beta+\beta\ln\beta$. This yields $U_*>0$ at $\beta<1$. The height of the potential barrier decreases with increasing β; the barrier disappears at $\beta=1$. At given β, the case of $A/2<G(U_*)$ corresponds to the repulsion from the potential barrier at a turning point U_1, for which $A/2=G(U_1)$. After that the particle moves to $U=-\infty$. Potentials $G(U)$ at different β are presented in Fig. 2. The case of $A/2<G(U_*)$ relates to nonphysical oscillations of solutions $U(x)$ with infinite amplitude. Therefore, the condition $A_c/2=G(U_*)$ determines the critical diffusion flux to the wire base $\sqrt{A_c}$, below which the wires cannot be grown by the surface diffusion. For fluxes lower than $\sqrt{A_c}$, the dominant fraction of adatoms cannot reach the wire top because of very efficient sidewall nucleation. The lateral growth dominates over the vertical one and the crystals grow in the form of islands rather than wires. The resulting morphology is a corrugated laterally overgrown surface instead of the expected anisotropic array. The curve $\sqrt{A_c}=\sqrt{2(1-\beta+\ln\beta)}$ in the $\sqrt{A}-\beta$ plane, shown in Fig. 3, separates the region of wire growth (above the curve) from the islanding region (below the curve). The decrease of the critical flux with β is well understood intuitively, because the direct impingement to the sidewalls at the wire neck promotes the vertical growth.

The wire shape is obtained in a simple analytical form in the case $\beta=0$, when the beam is strictly perpendicular to the surface. This is a standard assumption in MBE [7,8]. At $\beta=0$, Eq. (17) can be integrated exactly,

$$U(x)=2\ln\left[\frac{\sinh[\alpha(x+x_0)]}{\sqrt{2}\alpha}\right], \tag{19}$$

where the constants are given by

$$\alpha=\frac{\sqrt{A-2}}{2},\quad x_0=-\frac{1}{2\alpha}\ln\left(\frac{\sqrt{1/2+\alpha^2}-\alpha}{\sqrt{1/2+\alpha^2}+\alpha}\right). \tag{20}$$

Inserting Eq. (19) into Eq. (13) and integrating, we obtain the exact solution for the wire shape $\rho(x,l)$. Below we present the resulting expression only in the case of $\nu=0$, when the diffusion-induced contribution to the vertical growth rate is much larger then the flux directly impinging the wire top,

$$\rho(x,l)=1+\frac{1}{2\sinh^2[\alpha(x+x_0)]}\ln\left(\frac{\cosh[\alpha(l+x_0)]}{\cosh[\alpha(x+x_0)]}\right). \tag{21}$$

The supersaturation of adatoms and the wire shape in normalized coordinates now depend on the only parameter $\sqrt{A}$. The cylinder to cone shape transformation, induced by the reduction in the supplying flux at the wire foot, is demonstrated in Fig. 4. The critical diffusion flux now equals $\sqrt{2}$. According to Eq. (20), $x_0\to\sqrt{2}$ at $\alpha\to 0$, and Eq. (21) is reduced to

$$\rho_c(x,l)=\frac{3}{4}+\frac{1}{4}\left(\frac{l+\sqrt{2}}{x+\sqrt{2}}\right)^2. \tag{22}$$

This function, shown as a dashed-dotted curve in Fig. 4, does not depend on any of the system parameters and is determined entirely by the form of model equations. The critical curve describes the limit case of the thickest possible wire of given length l that can be grown by the surface diffusion. The radius of the wire base $\rho(0,l)$ scales with l as l^2 at large l so that the lateral growth is much faster than the vertical one. The growth of a wire of shape (22) with a finite length l requires infinite time.

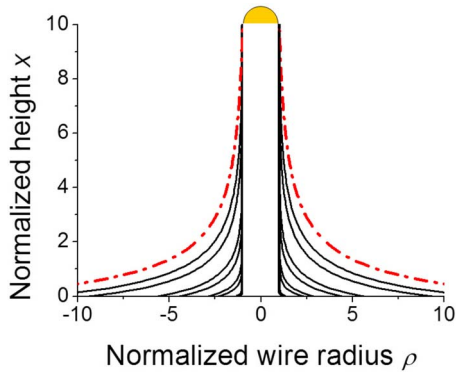

FIG. 4. (Color online) Wire shape $\rho(x,l)$ as given by Eq. (21) for fixed $l=10$ and different $\sqrt{A}=13$ (bold cylinder), 7.8, 4.5, 3.3, 2.4, 1.9, 1.5, and $\sqrt{2}$. The lateral growth rate increases as $\sqrt{A}$ decreases. The dashed-dotted curve is the critical curve.

IV. TEMPERATURE DEPENDENCE

The temperature behavior of wire shape is dictated by the temperature dependence of the diffusion flux and the effective diffusion length on the sidewalls. Although it is not essential, we restrict the following analysis to the case $\beta=0$, when the wire radius $\rho(x,l)$ is given by simple equation (21). As shown in Ref. [22], the boundary condition at the wire foot of form (6) yields $j_0/(2\pi R_0)=\varepsilon V/(\Omega P_W)$, where P_W is the total perimeter of the wire bases per unit surface area. At a small desorption from the surface, the parameter ε can be estimated as $\varepsilon=P_W/(P_W+P_I)$, where P_I is the appropriately averaged perimeter of islands emerging in the surface layer. The latter depends on the temperature T and the flux V as $P_I \propto V \exp[(3\Lambda/2+E_D)/k_BT]$, with Λ being the specific condensation heat and E_D the diffusion barrier for adatoms [22]. At otherwise similar growth conditions, P_I increases at lower T because of the higher density of islands [22,24]. To estimate the unknown supersaturation at the wire foot, we use the model of an amorphous crystal growing uniformly in all directions. In this approximation the lateral growth rate at $z=0$ equals the vertical growth rate of the surface layer itself: $V_R(0)\cong V_s=(1-\varepsilon)V$. Using this in Eqs. (7) and (8) at $\eta=\eta_0$, with logarithmic accuracy we obtain $\eta_0 \cong \exp(a/3 \ln\{h/[(1-\varepsilon)V\tau_D]\})$. This exponent contains the ratio of two very large values—the thermodynamic constant a to the logarithmic ratio of the macroscopic deposition time h/V and the microscopic time of island growth τ_D. The latter is defined as $\tau_D=t_D/\theta_{eq}$, where t_D is the diffusion time [such that the diffusion coefficient $D=\Omega/(ht_D)$] and $\theta_{eq}=(\Omega/h)n_{eq}$ is the equilibrium adatom coverage of the surface [10]. Substitution of this expression for η_0 into Eqs. (14) and (15) together with the conventional temperature dependences $t_D=\nu_D^{-1}\exp(E_D/k_BT)$ and $\theta_{eq}=\exp(-\Lambda/k_BT)$ [21–24] leads to

$$L_* \cong \left(\frac{3\Omega\eta_0}{4(1-\varepsilon)\Gamma V\tau_D}\right)^{1/2} \propto \frac{1}{\sqrt{V}}\exp\left(-\frac{(E_D+\Lambda)}{k_BT}\right), \tag{23}$$

$$\sqrt{A} \cong \frac{1}{L_* P_I} \propto \frac{1}{\sqrt{V}}\exp\left(-\frac{(E_D+2\Lambda)}{2k_BT}\right). \tag{24}$$

When deriving these semiquantitative expressions, we again assume that the characteristics of the surface layer and the sidewalls at the wire foot are approximately the same. Equations (23) and (24) demonstrate that the diffusion length and the flux decrease at a lower temperature as the Arrhenius exponents, also scaling at increasing flux as $1/\sqrt{V}$. Therefore, the critical diffusion flux relates to a certain minimum temperature, below which the wires cannot be grown.

V. THEORY AND EXPERIMENT

In this section we use the described model for fitting our experimental data obtained for Au-assisted MBE of GaAs and GaP wires. Growth experiments were performed in a Riber 32 MBE machine equipped with the solid source of Ga atoms and the cracker sources to produce dimers of As (P). We used $(111)B$ substrates activated by an Au layer of approximately 1 nm equivalent thickness, deposited in the MBE vacuum chamber and annealed before growth. In all growth runs, the deposition rate V was fixed to 0.2 nm/s, the V/III flux ratio was set to 3, while the substrate temperature T was varied. More experimental details can be found in Refs. [16,17]. In all cases we observed pronounced lateral growth and the cylinder to cone shape modification at sufficiently low T. In the case of InAs nanowires grown by Au-assisted metal organic vapor pressure epitaxy, a similar effect was described in Ref. [26]: the nanowires had an approximately cylindrical shape at $T=480$ °C and a conical shape with a much smaller length at $T=420$ °C. It is noteworthy that our GaAs and GaP nanowires are obtained at T well above the eutectic melting point of bulk Au-Ga alloy (339.4 °C [27]) and therefore grow by the conventional vapor-liquid-solid mechanism [13]. InAs wires of Ref. [26] were grown below the melting point of bulk Au-In alloy (454.3 °C [27]), so that their formation could proceed via the vapor-solid-solid mechanism [28]. However, in both cases, the wire growth is controlled by the adatom diffusion [7,28]. Since the supersaturation generally decreases with the height, the physical reason for the shape modification should remain qualitatively the same for both systems, regardless of the state of catalyst on the wire top.

Figures 5 and 6 demonstrate the scanning electron microscopy (SEM) images of GaAs and GaP wires grown at different T. GaAs wires shown in Fig. 5(b) grow with approximately constant radius up to approximately 3 microns of their length and then taper due to the desorption of some Ga atoms, as discussed in the Introduction. When T is below 500 °C, the wires adopt a specific conical shape, shown in Fig. 5(a) for $T=420$ °C. Similar growth behavior is observed for GaP wires, where the shape modification demonstrated by Fig. 6 occurs at T decreasing from 580 to 450 °C, although the drop radius R_d is now three times smaller. Figure 7 shows the typical example of experimental and theoretical wire shapes $R(z)$ at low T. The GaAs wire chosen for comparison with calculations is highlighted in the SEM image in Fig. 5. The error bars indicate uncertainty in the measured

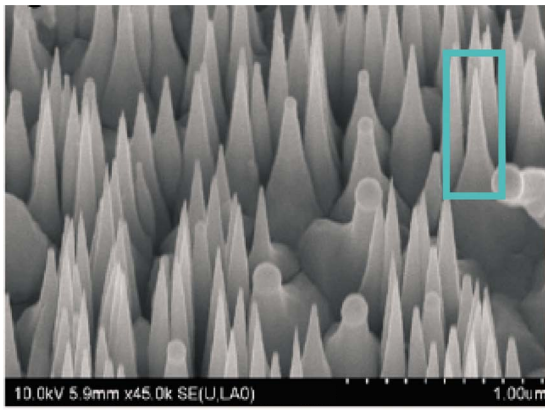

(a)

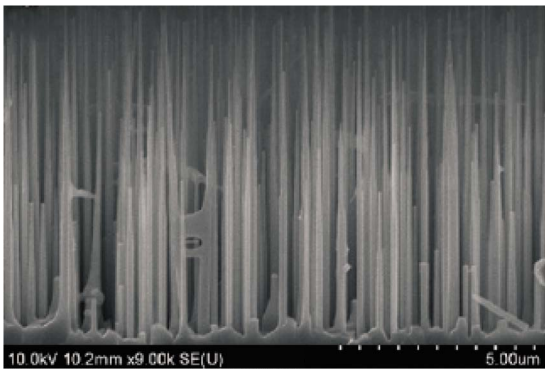

(b)

FIG. 5. (Color online) SEM images of MBE-grown GaAs wires. The growth was performed at (a) 420 °C (45° tilted view) and (b) 580 °C (cross view).

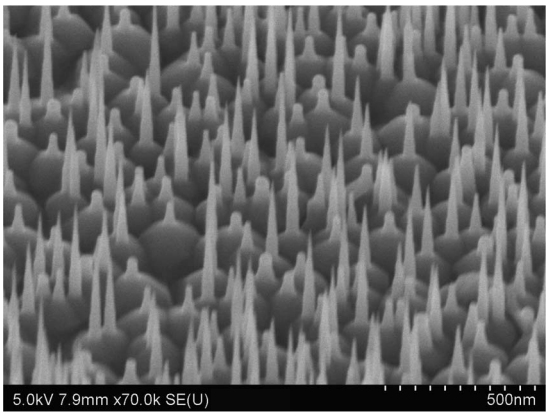

(a)

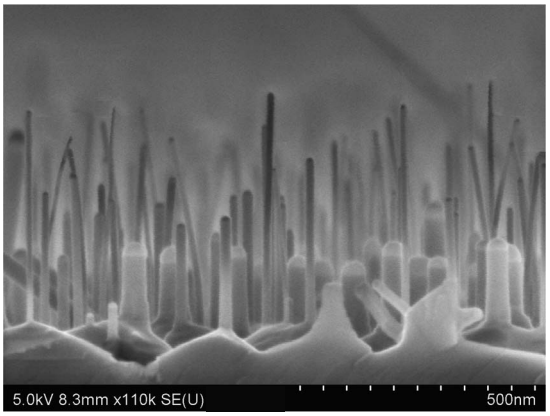

(b)

FIG. 6. SEM images of GaP wires grown by MBE at (a) 420 °C (45° tilted view) and (b) 580 °C (cross view).

$R(z)$ dependences of different wires with the same length, obtained from the statistical analysis of SEM image. Theoretical curves are obtained from the numerical solution of Eqs. (11)–(13). Normalized coordinates (ρ,x) are then transformed into (R,z) by fitting the value of L_* at known R_d. The best fits to the experimental $R(z)$ dependences are obtained at the values of parameters given in Table I, where the MBE growth conditions are also presented. We find that the value of $\upsilon \approx 0$ is a good approximation, i.e., the direct impingement to the drop can be safely neglected. In both cases, the best fit to the experimental data is obtained at low values of $\sqrt{A}=1.13-1.2$, demonstrating that the growth parameters are quite close to the critical flux. This is in line with our experimental findings, because regular epitaxial wires can hardly be observed at T lower than 420 °C for GaAs and 450 °C for GaP. The value of $\beta=0.525$, obtained from the best fit in both cases, at the incident angle $\theta_0=20°$, provides the estimate for $V_R(0)=0.07$ nm/s. This gives a reasonable value of the substrate growth rate at approximately 35% of the deposition rate. Finally, in all our simulations of different GaAs and GaP wires with pronounced conical shape the effective diffusion length on the sidewalls was not larger than 300 nm, i.e., at least ten times smaller than the diffusion length of Ga atoms on the GaAs(110) surface at 580 °C, limited by desorption.

In conclusion, we have shown that the shape modification of III-V nanowires can be modeled by the nonlinear equation for the adatom supersaturation, changing due to the direct impingement, diffusion, and nucleation. The obtained solution provides the phase diagram, separating the domains of wire growth and two-dimensional island growth. Nucleation on the sidewalls becomes pronounced at sufficiently low temperatures. The model equations demonstrate reasonable

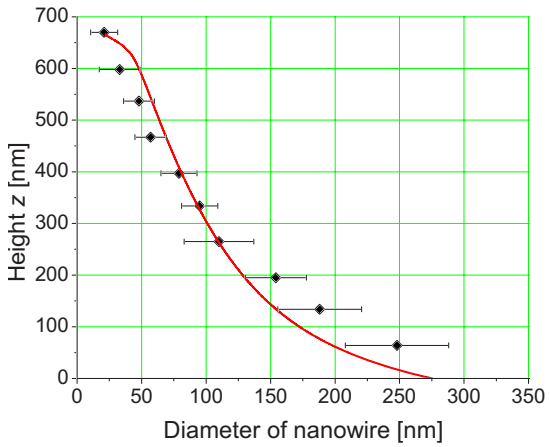

FIG. 7. (Color online) Experimental (black squares) and theoretical (solid line) wire shape $2R(z)$ for the GaAs wire shown in Fig. 5(a).

TABLE I. Growth conditions and fitting parameters of conical III-V wires.

Wire material	Surface temperature T (°C)	Drop radius R_d (nm)	Wire length L (nm)	$\sqrt{A}$	β	Diffusion length L_* (nm)
GaAs	420	30	670	1.13	0.525	160
GaP	450	10	165	1.2	0.525	100

correlation with our experimental data on the GaAs and GaP wires, grown by the Au-assisted MBE. Fitting theoretical and experimental wire shapes allows us to estimate some important parameters of the growth process. In particular, we have found that the effective diffusion length of Ga atoms at the wire foot at low T is limited entirely by the nucleation and is as small as 160 nm for GaAs wires at $T=420$ °C and 100 nm for GaP wires at $T=450$ °C. We now intend to model more complex geometrical shapes with an abrupt change of wire radius, observed in the case of InAs wires [28], account for the atomic structure of the lateral facets, and consider the effect of lateral growth on the formation and properties of heterostructured III-V nanowires.

ACKNOWLEDGMENTS

This work was partially supported by the Russian Federal Agency for Science and Innovation, SANDiE Network of Excellence of European Commission, different grants of the Russian Academy of Sciences and the Russian Foundation for Basic Research.

[1] M. S. Gudiksen, L. J. Lauhon, J. Wang, D. C. Smith, and C. M. Lieber, Nature (London) **415**, 617 (2002).
[2] M. T. Björk, B. J. Ohlsson, T. Sass, A. I. Persson, C. Thelander, M. H. Magnusson, K. Deppert, L. R. Wallenberg, and L. Samuelson, Appl. Phys. Lett. **80**, 1058 (2002).
[3] Y. Cui and C. M. Lieber, Science **91**, 851 (2000).
[4] F. Patolsky, G. Zheng, O. Hayden, M. Lakadamyali, X. Zhuang, and C. M. Lieber, Proc. Natl. Acad. Sci. U.S.A. **101**, 14017 (2004).
[5] L. Schubert, P. Werner, N. D. Zakharov, G. Gerth, F. M. Kolb, L. Long, U. Gösele, and T. Y. Tan, Appl. Phys. Lett. **84**, 4968 (2004).
[6] W. Seifert, M. Borgstrom, K. Deppert, K. A. Dick, J. Johansson, M. W. Larsson, T. Martensson, N. Skold, C. P. T. Svensson, B. A. Wacaser, L. R. Wallenberg, and L. Samuelson, J. Cryst. Growth **272**, 211 (2004).
[7] V. G. Dubrovskii, G. E. Cirlin, I. P. Soshnikov, A. A. Tonkikh, N. V. Sibirev, Yu. B. Samsonenko, and V. M. Ustinov, Phys. Rev. B **71**, 205325 (2005).
[8] J. C. Harmand, G. Patriarche, N. Péré-Laperne, M.-N. Mérat-Combes, L. Travers, and F. Glas, Appl. Phys. Lett. **87**, 203101 (2005).
[9] M. C. Plante and R. R. LaPierre, J. Cryst. Growth **286**(2), 394 (2006).
[10] V. G. Dubrovskii, N. V. Sibirev, G. E. Cirlin, J. C. Harmand, and V. M. Ustinov, Phys. Rev. E **73**, 021603 (2006).
[11] F. Glas and J. C. Harmand, Phys. Rev. B **73**, 155320 (2006).
[12] A. I. Persson, L. E. Fröberg, S. Jeppesen, M. T. Björk, and L. Samuelson, J. Appl. Phys. **101**, 034313 (2007).
[13] R. S. Wagner and W. C. Ellis, Appl. Phys. Lett. **4**, 89 (1964).
[14] E. I. Givargizov, *Highly Anisotropic Crystals* (Springer, Berlin, 1987).
[15] R. K. Debnath, R. Meijers, T. Richter, T. Stoica, R. Calarco, and H. Lüth, Appl. Phys. Lett. **90**, 123117 (2007).
[16] M. Tchernycheva, J. C. Harmand, G. Patriarche, L. Travers, and G. E. Cirlin, Nanotechnology **17**, 4025 (2006).
[17] J. C. Harmand, M. Tchernycheva, G. Patriarche, L. Travers, F. Glas, and G. Cirlin, J. Cryst. Growth **304**, 504 (2007).
[18] F. M. Kolb, H. Hofmeister, R. Scholz, M. Zacharias, U. Gosele, D. D. Ma, and S.-T. Lee, J. Electrochem. Soc. **151**, G472 (2004).
[19] V. G. Dubrovskii, I. P. Soshnikov, G. E. Cirlin, A. A. Tonkikh, Yu. B. Samsonenko, N. V. Sibirev, and V. M. Ustinov, Phys. Status Solidi B **241**, R30 (2004).
[20] D. Kashchiev, *Nucleation: Basic Theory with Applications* (Butterworth Heinemann, Oxford, 2000).
[21] V. G. Dubrovskii and N. V. Sibirev, J. Cryst. Growth **304**, 504 (2007).
[22] V. G. Dubrovskii, N. V. Sibirev, R. A. Suris, G. E. Cirlin, J. C. Harmand, and V. M. Ustinov, Surf. Sci. **601**, 4395 (2007).
[23] V. G. Dubrovskii and N. V. Sibirev, Phys. Rev. E **70**, 031604 (2004).
[24] S. A. Kukushkin and A. V. Osipov, Prog. Surf. Sci. **51**, 1 (1996).
[25] T. Takebe, M. Fujii, T. Yamamoto, K. Fujita, and T. Watanabe, J. Appl. Phys. **81**, 7273 (1997).
[26] K. A. Dick, K. Deppert, T. Mårtensson, B. Mandl, L. Samuelson, and W. Seifert, Nano Lett. **5**, 761 (2005).
[27] *Binary Alloy Phase Diagrams*, edited by T. B. Massalski, 2nd ed. (ASM International, Metals Park, OH, 1990), Vol. 1.
[28] M. Tchernycheva, L. Travers, G. Patriarche, J. C. Harmand, G. E. Cirlin and V. G. Dubrovskii, J. Appl. Phys. **102**, 094313 (2007).